Stability of the perovskite structure and possibility of the transition to the post-perovskite structure in $CaSiO_3$, $FeSiO_3$, $MnSiO_3$ and $CoSiO_3$

Kiyoshi Fujino[a, b]*, Daisuke Nishio-Hamane[a, c], Keisuke Suzuki[a], Hiroyuki Izumi[a], Yusuke Seto[a, d], Takaya Nagai[a]

[a]Department of Natural History Sciences, Hokkaido University, Sapporo 060-0810, Japan

[b]Geodynamics Research Center, Ehime University, Matsuyama 790-8577, Japan

[c]Institute for Solid State Physics, The University of Tokyo, Kashiwa 277-8581, Japan

[d]Department of Earth and Planetary Sciences, Kobe University, Kobe 657-8501, Japan

Abstract

High pressure and high temperature experiments on $CaSiO_3$, $FeSiO_3$, $MnSiO_3$ and $CoSiO_3$ using a laser-heated diamond anvil cell combined with synchrotron X-ray diffraction were conducted to explore the perovskite structure of these compounds and the transition to the post-perovskite structure. The experimental results revealed that $MnSiO_3$ has a perovskite structure from relatively low pressure (ca. 20 GPa) similarly to $CaSiO_3$, while the stable forms of $FeSiO_3$ and $CoSiO_3$ are mixtures of mono-oxide (NaCl structure) + high pressure polymorph of SiO_2 even at very high pressure and temperature (149 GPa and 1800 K for $FeSiO_3$ and 79 GPa and 2000 K for $CoSiO_3$). This strongly suggests that the crystal field stabilization energy (CFSE) of Fe^{2+} with six 3d electrons and Co^{2+} with seven 3d electrons at the octahedral site of mono-oxides favors a mixture of mono-oxide + SiO_2 over perovskite where Fe^{2+} and Co^{2+} would occupy the distorted dodecahedral sites having a smaller CFSE (Mn^{2+} has five 3d electrons and has no CFSE). The structural characteristics that the orthorhombic distortion of $MnSiO_3$ perovskite decreases with pressure and the tolerance factor of $CaSiO_3$ perovskite (0.99) is far from the orthorhombic range suggest that both $MnSiO_3$ and $CaSiO_3$ perovskites will not transform to the $CaIrO_3$-type

* Corresponding author. Tel.: +81-(0)89-927-8150; fax: +81-(0)89-927-8167.
E-mail address: fujino@sci.ehime-u.ac.jp

post-perovskite structure even at the Earth's core-mantle boundary conditions, although $CaSiO_3$ perovskite has a potentiality to transform to the $CaIrO_3$-type post-perovskite structure at still higher pressure as long as another type of transformation does not occur.

Keywords: silicate perovskite; $CaSiO_3$; $MnSiO_3$; $FeSiO_3$; $CoSiO_3$; crystal field stabilization energy; tolerance factor; $CaIrO_3$-type post-perovskite

1. Introduction

In the series of silicate compounds, $MgSiO_3$, $CoSiO_3$, $FeSiO_3$, $MnSiO_3$ and $CaSiO_3$, it had been known that only $MgSiO_3$ and $CaSiO_3$ have a perovskite structure at high pressure and high temperature, and very recently, $MnSiO_3$ was also found to have a perovskite structure (Fujino et al., 2008). However, there has been no report that $CoSiO_3$ and $FeSiO_3$ compounds have a perovskite structure at high pressure, although the tolerance factors of these compounds (0.904 for $CoSiO_3$ and 0.912 for $FeSiO_3$) are between those of $MgSiO_3$ (0.900) and $CaSiO_3$ (0.990), where the tolerance factor $t = (r_A + r_O) / [\sqrt{2}\,(r_B + r_O)]$ and r_A, r_B and r_O are the ionic radii of eightfold A cation, sixfold B cation and oxygen, respectively, in ABO_3 compounds (Goldschmidt, 1926) (here the ionic radii were taken from Shannon, 1976).

The stable form of $FeSiO_3$ at ambient pressure, Fe_2SiO_4 (olivine) + SiO_2 (quartz), transforms to $FeSiO_3$ (orthopyroxene) and to $FeSiO_3$ (clinopyroxene) with increasing pressure (Akimoto et al., 1965). $FeSiO_3$ (clinopyroxene) decomposes into Fe_2SiO_4 (γ–spinel) + SiO_2 (stishovite) at 9 GPa and 1200 K (Akimoto, 1970), and it further transforms to FeO with a rock salt structure (B1 structure) + SiO_2 (stishovite) at 20 GPa and 1800 K (Ming and Bassett, 1975). However, the further phase transformation of $FeSiO_3$ at still higher pressure has not been reported except for the rhombohedral distortion of FeO and the polymorphic phase transition of SiO_2.

$CoSiO_3$ does not exist as a stable single compound at ambient pressure. The stable assemblage of Co_2SiO_4 (olivine) + SiO_2 (quartz) at ambient pressure transforms to $CoSiO_3$ (orthopyroxene) and to $CoSiO_3$ (clinopyroxene) with increasing pressure (Akimoto et al., 1965). It decomposes into Co_2SiO_4 (γ-spinel) + SiO_2 (stishovite) at 10 GPa and 1273 K (Ringwood, 1970), and further

decomposes into CoO (B1) + SiO_2 (stishovite) at 17 GPa and 2000 K (Ito, 1975). So far, the phase transformation at still higher pressure has not been reported.

Meanwhile, $MnSiO_3$ has many high pressure polymorphs at pressures up to around 20 GPa, starting from rhodonite to pyroxmangite, to clinopyroxene, and to tetragonal garnet (Akimoto and Syono, 1972; Fujino et al., 1986). Regarding the stable form of $MnSiO_3$ at higher pressures, Liu (1976) reported that $MnSiO_3$ garnet decomposes into MnO (B1) + SiO_2 (stishovite) at 26 GPa and from 1673 to 2073 K, and Ito and Matsui (1977) also reported the stable assemblage of the same oxide mixture at 22 GPa and 1273 K. However, our recent study showed that $MnSiO_3$ has also a perovskite structure similar to $MgSiO_3$ and $CaSiO_3$, at the lower temperature side of MnO (B1) + SiO_2 (stishovite) (Fujino et al., 2008).

If $FeSiO_3$ and $CoSiO_3$ do not have a perovskite structure even at higher pressure, then, the other factor than the tolerance factor would control the stability of the perovskite structure of $FeSiO_3$ and $CoSiO_3$. One of the possible candidates will be the crystal field stabilization energy (CFSE) of Fe^{2+} and Co^{2+} with unfilled 3d electrons (six 3d electrons for Fe^{2+} and seven 3d electrons for Co^{2+}), because Mn^{2+} has five 3d electrons and has no CFSE. CFSE of the octahedral site of mono-oxides is large compared to that of the dodecahedral site of perovskites (Burns, 1993), and would favor a mixture of mono-oxide + SiO_2 over a perovskite structure.

Another interesting point in the above series of silicate compounds is that $MgSiO_3$ perovskite further transforms to the $CaIrO_3$-type post-perovskite structure at around 125 GPa and 2500 K (Murakami et al., 2004; Oganov and Ono, 2004), while there has been no report of the phase transition of the other silicate perovskites to the $CaIrO_3$-type post-perovskite structure at very high pressure. Then, what factors control the phase transition of the perovskite structure to the $CaIrO_3$-type post-perovskite structure? Are there any other silicate perovskites that transform to the $CaIrO_3$-type post-perovskite structure?

To clarify the above problems, we have examined the high pressure phase relations of $CaSiO_3$, $FeSiO_3$, $MnSiO_3$ and $CoSiO_3$ using a laser-heated diamond anvil cell combined with synchrotron

X-ray diffraction. Here, the focus is laid on what factors control the stability of perovskite structure and the phase transition to the $CaIrO_3$-type post-perovskite structure in $CaSiO_3$, $MnSiO_3$, $FeSiO_3$ and $CoSiO_3$.

2. Experimental

2.1. Laser-heated diamond anvil cell experiments

The high pressure and high temperature experiments to synthesize the high pressure forms of respective compounds were carried out using an YLF or YAG laser-heated diamond anvil cell (LHDAC). The synthesis conditions were 30 - 149 GPa and 1600 - 2100 K for $CaSiO_3$-$FeSiO_3$, 15 - 85 GPa and 1200 - 2600 K for $MnSiO_3$ and 50, 79 GPa and 2000 K for Co_2SiO_4. The starting materials for the LHDAC experiments were gel (+ crystal) for $CaSiO_3$-$FeSiO_3$, synthetic $MnSiO_3$ rhodonite for $MnSiO_3$, and synthetic Co_2SiO_4 olivine for $CoSiO_3$. The reason why Co_2SiO_4 olivine was used as a starting material for $CoSiO_3$ is because the $CoSiO_3$ compound is not stable as a single phase at ambient pressure. A small amount of Au or Pt was added to some samples to determine pressure in high pressure and high temperature X-ray diffraction experiments by the equation of state (Anderson et al., 1989 for Au and Holmes et al., 1989 for Pt). Diamond anvils with a 300 or 200 μm culet were used for pressures less than 100 GPa, while beveled diamonds with an inner culet of 150 μm and an outer culet of 450 μm were used for pressures higher than 100 GPa. The samples were loaded into the hole of 50 - 100 μm diameter in a Re gasket (the original thickness was 0.25 mm) and sandwiched by NaCl pellets in a DAC. Samples in a DAC were heated from both sides with an YLF or YAG laser. Temperature was measured by the spectroradiometric method (Watanuki et al., 2001). Pressure at room temperature was measured by the ruby fluorescence technique (Mao et al., 1986), by the Raman spectral shift of diamond (Akahama and Kawamura, 2005) or by the equation of state of NaCl (Sata et al., 2002). Further details for $MnSiO_3$ are described in Fujino et al. (2008), and those for $CaSiO_3$-$FeSiO_3$ will be described elsewhere (Fujino et al., in preparation).

2.2. Synchrotron X-ray diffraction experiments

Angle-dispersive X-ray diffraction experiments of $CaSiO_3$-$FeSiO_3$, $MnSiO_3$ and Co_2SiO_4 at room temperature were performed at BL-13A (wave length of 0.42 - 0.43 Å) and BL-18C (wave length of ~ 0.61 Å) of Photon Factory, KEK, and those at high pressure and high temperature were carried out at BL-10XU (wave length of 0.41 - 0.42 Å) of SPring-8 of the Japan Synchrotron Radiation Research Institute. Monochromatic X-ray incident beams were collimated to 15 - 20 μm (BL-13A and BL-18C), and to 20 - 30 μm (BL-10XU). Diffraction patterns were recorded on an imaging plate (3000 x 3000 pixels for BL-13A and BL-10XU and 2000 x 2500 pixels for BL-18C with a pixel size of 100 μm x 100 μm) at all the beam lines. The exposure times were 10 - 60 min at BL-13A, 30 - 120 min at BL-18C and ~ 5 min at BL-10XU. Two-dimensional X-ray diffraction images on the imaging plates were integrated as a function of 2θ in order to obtain the conventional one-dimensional diffraction profiles and analyzed using the software PIP (Fujisawa and Aoki, 1998) or IPA and PDI (Y. Seto, available from http://www2.kobe-u.ac.jp/~seto/). The typical diffraction patterns obtained for the compounds $FeSiO_3$, $CaFeSi_2O_6$, $MnSiO_3$ and Co_2SiO_4 at high pressure and high temperature or high pressure and room temperature quenched from high temperature are presented in Fig. 1.

3. High pressure phase relations

$CaSiO_3$ and $FeSiO_3$

In the system $CaSiO_3$-$FeSiO_3$ at 30 - 149 GPa and 1600 - 2100 K (Fujino et al., in the preparation), the stable assemblage of the end member $FeSiO_3$ was a mixture of FeO (B1 structure) + high pressure polymorph of SiO_2 (stishovite, $CaCl_2$-type or α-PbO_2-type with increasing pressure) up to 117 GPa and 2100 K (Fig. 1(a)). Further, the stable assemblage of the intermediate composition $CaFeSi_2O_6$ was a mixture of Fe-bearing $CaSiO_3$ perovskite + FeO (B1 structure) + high-pressure polymorph of SiO_2 (stishovite, $CaCl_2$-type or α-PbO_2-type with increasing pressure) up to 149 GPa and 1800 K (Fig. 1(b)). These results indicate that $CaSiO_3$ has a perovskite structure up to 149 GPa and it does not transform to the post-perovskite structure

even at this pressure, while the high pressure form of $FeSiO_3$ is a mixture of FeO (B1) + high pressure polymorph of SiO_2 and $FeSiO_3$ perovskite does not become stable up to 149 GPa. All the Fe-bearing $CaSiO_3$ perovskite phases showed cubic symmetry (space group Pm3m) at high pressure and high temperature, but showed tetragonal symmetry (exact space group could not be determined) at high pressure and room temperature. The c/a ratio (<1) of the refined cell parameters of present Fe-bearing $CaSiO_3$ perovskite at high pressure and room temperature decreases with pressure (Fujino et al., in the preparation) in the same way as pure $CaSiO_3$ perovskite (Ono et al., 2004). These results indicate that the tetragonal distortion of $CaSiO_3$ perovskite increases with pressure.

$MnSiO_3$

Our recent X-ray diffraction experiments at high pressure and high temperature up to 85 GPa and 2600 K (Fujino et al., 2008) revealed that at the higher temperature region $MnSiO_3$ garnet decomposes into an assemblage of MnO (B1) + SiO_2 (stishovite), while at the lower temperature region $MnSiO_3$ garnet directly transforms to the perovskite structure from relatively low pressure around 20 GPa as shown in Fig. 2. The triple point of the three stable regions of garnet, MnO + SiO_2 and perovskite is ca. 20 GPa and 1200 K. $MnSiO_3$ perovskite showed orthorhombic symmetry (space group Pbnm) both at high temperature and room temperature under high pressure (Fig. 1(c)). The refined cell parameters of $MnSiO_3$ perovskite demonstrate that the *a* axis approaches the *b* axis with pressure, while the $\sqrt{2}a/c$ ratio (= 1 for cubic) remains nearly constant (<1) (Fig. 4 in Fujino et al., 2008). This indicates that the orthorhombic distortion of $MnSiO_3$ perovskite decreases with pressure and $MnSiO_3$ perovskite approaches tetragonal perovskite.

$CoSiO_3$

The X-ray diffraction patterns of Co_2SiO_4 were all taken at room temperature quenched from high temperature. The diffraction pattern of Co_2SiO_4 at 50 GPa and room temperature quenched

from 2000 K showed the mixed peaks of CoO (B1) + SiO_2 (stishovite) (Fig. 1(d)). Its diffraction pattern at 79 GPa and room temperature quenched from 2000 K turned to be the mixed peaks of CoO (this seems to be rhombohedrally distorted from B1 as Guo et al., 2002, reports) + SiO_2 ($CaCl_2$-type). The variation of the diffraction peaks of CoO with increasing pressure at room temperature suggests that CoO has a B1 structure at high pressure and high temperature like FeO and MnO (Kondo et al., 2000, 2004). These results indicate that the stable form of $CoSiO_3$ is CoO (B1) + high pressure polymorph of SiO_2, not perovksite at high pressure and high temperature up to 79 GPa and 2000 K.

4. Stability of the perovskite structure and possibility of the phase transition to post-perovskite

4.1. Stability of the perovskite structure in $FeSiO_3$, $MnSiO_3$ and $CoSiO_3$

High pressure phase studies of $FeSiO_3$, $MnSiO_3$ and $CoSiO_3$ demonstrated that $MnSiO_3$ has a perovskite structure from relatively low pressure as 20 GPa, while $FeSiO_3$ and $CoSiO_3$ do not have a perovskite structure even at very high pressure. Table 1 summarizes the transformation pressures of the selected silicate compounds to the perovskite structure at 1200 K. Here, the polymorphic phase transition pressures to the perovskite structure were selected for $MgSiO_3$ and $MnSiO_3$, while the transformation pressure of Ca_2SiO_4 (larnite) + $CaSi_2O_5$ (titanite structure) to the perovskite structure was selected for $CaSiO_3$, since there is no polymorphic transition to the perovskite structure for $CaSiO_3$. Although the types of transformation are different among $MgSiO_3$, $MnSiO_3$ and $CaSiO_3$, their transformation pressures are relatively low, 13 – 25 GPa at 1200 K. On the other hand, $FeSiO_3$ and $CoSiO_3$ do not have a perovskite structure even at very high pressure beyond ~ 80 GPa. This fact is well explained by the CFSE of the transition metals with unfilled 3d electrons ($\neq$five) at the octahedral site of mono-oxides with a B1 structure. Fig. 3 illustrates the assumed CFSEs of Fe^{2+} and Co^{2+} at the octahedral site of mono-oxides with a B1 structure and the dodecahedral site of silicate perovskites. Compared to the CFSEs at the octahedral site of

mono-oxides, those at the distorted dodecahedral site of silicate perovskites are smaller (Burns, 1993) and further separated. Therefore, the CFSEs of both Fe^{2+} and Co^{2+} favor a mixture of mono-oxide + SiO_2 over a perovskite structure, while the mixture of MnO + SiO_2 is not favored because no CFSE is expected for Mn^{2+} with five 3d electrons.

The above argument was discussed under the assumption that the spin states of the transition metals are high spin. When the spin states of the transition metals at the octahedral site of mono-oxides become low spin at very high pressure, the mixtures of mono-oxide + SiO_2 will be further stabilized by the large volume reductions induced by the high spin - low spin transitions of Fe^{2+} and Co^{2+} at the octahedral site of mono-oxides. Even for $MnSiO_3$ the mixture of MnO + SiO_2 may be favored compared to perovskite because Mn^{2+} with five 3d electrons at the octahedral site also has a large volume reduction by the high spin - low spin transition.

4.2. Possibility of the transition to the $CaIrO_3$-type post-perovskite structure in $CaSiO_3$ and $MnSiO_3$

Among the silicate perovskites of $MgSiO_3$, $CaSiO_3$ and $MnSiO_3$, only $MgSiO_3$ perovskite further transforms to the $CaIrO_3$-type post-perovkite structure. How about the possibility of the post-perovskite phase of $CaSiO_3$ and $MnSiO_3$? Fig.4 shows the Goldschmidt diagram of $A^{2+}B^{4+}O_3$ compounds. All the compounds in this diagram have a perovskite structure at high pressure. Among these compounds, so far, only 4 compounds (solid circles), $MgSiO_3$, $MgGeO_3$, $MnGeO_3$ and $CaIrO_3$, transform to the $CaIrO_3$-type post-perovskite structure (Murakami et al., 2004; Oganov and Ono, 2004; Hirose and Fujita, 2005; Hirose et al., 2005; Tateno et al., 2006). In this diagram, the compounds marked by solid symbols mean that their distortions increase with pressure, while the compounds marked by open symbols mean that their distortions decrease with pressure (Tateno et al., 2006). With the above 4 compounds which transform to the $CaIrO_3$-type post-perovskite structure, 1) their tolerance factors are between 0.8 and 0.9, and 2) all their orthorhombic distortions increase with pressure. Therefore, these two criteria seem to be the

necessary conditions to transform to the $CaIrO_3$-type post-perovksite structure. However, although $CaTiO_3$, $CdTiO_3$, $MnTiO_3$ and $CaSnO_3$ marked by solid triangle satisfy these two criteria, Tateno et al. (2006) report that these compounds transform to the other structures than $CaIrO_3$-type post-perovskite. So, still the other factors may be necessary to constrain the compounds which transform to the $CaIrO_3$-type post-perovskite structure. In any case, from these criteria, we can expect that $MnSiO_3$ will not transform to the $CaIrO_3$-type post-perovskite structure even at higher pressure because its orthorhombic distortion decreases with pressure. In the case of $CaSiO_3$, we also think that this will not transform to the $CaIrO_3$-type post-perovskite structure even at the core-mantle boundary conditions because its tolerance factor (0.99) is much larger than 0.8-0.9. However, considering that its tetragonal distortion increases with pressure, $CaSiO_3$ may have a potentiality to transform to the $CaIrO_3$-type post-perovskite structure at still higher pressure, if another type of transformation does not occur.

5. Summary

In addition to $MgSiO_3$ and $CaSiO_3$, $MnSiO_3$ also has a perovskite structure from relatively low pressure, while $FeSiO_3$ and $CoSiO_3$ do not have a perovskite structure and instead, mixtures of mono-oxide + SiO_2 are stable up to very high pressure. This strongly suggests that the CFSEs of Fe^{2+} (six 3d electrons) and Co^{2+} (seven 3d electrons) at the octahedral site of mono-oxides favor mono-oxide + SiO_2 over perovskite. Mn^{2+} has five 3d electrons and has no CFSE in the high spin state. When high spin-low spin transition occurs in these transition metals at the octahedral site of mono-oxides at high pressure, $FeSiO_3$ and $CoSiO_3$ will further, and even $MnSiO_3$ may, favor mono-oxide + SiO_2 by the large volume reduction induced by the high spin – low spin transition.

The orthorhombic distortion of $MnSiO_3$ perovskite decreases with pressure, while the tetragonal distortion of $CaSiO_3$ perovskite increases with pressure. However, the tolerance factor of $CaSiO_3$ (0.99) is far from 0.8-0.9 where, so far, the transition to $CaIrO_3$-type post-perovskite occurs. These characters of both $MnSiO_3$ and $CaSiO_3$ perovskites at high pressure suggest that

both of them will not transform to the $CaIrO_3$-type post-perovskite structure at the core-mantle boundary conditions, although $CaSiO_3$ perovskite has a potentiality to transform to the $CaIrO_3$-type post-perovskite structure at still higher pressure, if another type of transformation does not occur.

Acknowledgements

The X-ray diffraction experiments were carried out at SPring-8 (proposal no. 2004B0127, 2005B0283, 2006A1459 and 2006B1373) and at KEK (proposal no. 2003G206 and 2005G143). We thank Y. Ohishi and N. Sata at Spring-8, and T. Kikegawa at KEK for their help in the X-ray diffraction experiments. This work was supported in part by a 21st Century COE Program on "Neo-Science of Natural History" (Program Leader: Hisatake Okada) financed by the Ministry of Education, Culture, Sports, Science and Technology, Japan, and also by the Grant-in-Aid (no. 18340167 and 18204040) by Japan Society for the Promotion of Science (JSPS).

References

Akahama, Y. and Kawamura, H., 2005. Raman study on the stress state of [111] diamond anvils at multimegabar pressure. J. Appl. Phys., 98, Art. No. 083523.

Akaogi, M., Yano, M., Tejima,Y., Iijima, M., and Kojitani, H., 2004. High-pressure transitions of diopside and wollastonite: phase equilibria and thermochemistry of $CaMgSi_2O_6$, $CaSiO_3$ and $CaSi_2O_5$-$CaTiSiO_5$ system. Phys. Earth Planet. Inter., 143-144, 145-156.

Akimoto, S., Katsura, T., Syono, Y., Fujisawa, H., and Komada, E., 1965. Polymorphic transition of pyroxenes $FeSiO_3$ and $CoSiO_3$ at high pressures and temperatures. J. Geophys. Res., 70, 5269-5278.

Akimoto, S., 1970. High-pressure synthesis of a “modified” spinel and some geophysical implications. Phys. Earth Planet. Inter., 3, 189-195.

Akimoto, S. and Syono, Y., 1972. High pressure transformations in $MnSiO_3$. Am. Mineral., 57,

76-84.

Anderson, O.L., Isaak, D.G., and Yamamoto, S., 1989. Anharmonicity and the equation of state for gold. J. Appl. Phys., 65, 1534-1543.

Burns, R.G., 1993. Mineralogical Applications of Crystal Field Theory. Cambridge University Press, Cambridge, p. 551.

Fujino, K., Momoi, H., Sawamoto, H., and Kumazawa, M., 1986. Crystal structure and chemistry of $MnSiO_3$ tetragonal garnet. Am. Mineral., 71, 781-785.

Fujino, K., Suzuki, K., Hamane, D., Seto, Y, Nagai, T., and Sata, N., 2008. High pressure phase relation of $MnSiO_3$ up to 85 GPa: Existence of $MnSiO_3$ perovskite. Am. Mineral., 93, 653-657.

Fujisawa, H. and Aoki, K., 1998. High pressure X-ray powder diffraction experiments and intensity analyses. Rev. High Pressure Sci. Technol., 8, 4-9.

Goldschmidt, 1926. Die Gesetze der Krystallochemie. Naturwissenschaften, 14, 477-485.

Guo, Q., Mao, H.K., Hu, J., Shu, J., and Hemley, R.J., 2002. The phase transitions of CoO under static pressure to 104 GPa. J. Phys. Condens. Matter, 14, 11369-11374.

Hirose, K. and Fujita, Y., 2005. Clapeyron slope of the post-perovskite phase transition in $CaIrO_3$. Geophys. Res.Lett., 32, L13313, doi:10.1029/2005GL023219.

Hirose, K., Kawamura, K., Ohishi, Y., Tateno, S., and Sata, N., 2005. Stability and equation of state of $MgGeO_3$ post-perovskite phase. Am. Mineral. 90, 262-265.

Holmes, N.C., Moriarty, J.A., Gathers, G.R., and Nellis, W.J., 1989. The equation of state of platinum to 660 GPa (6.6 Mbar). J. Appl. Phys., 66, 2962-2967.

Ito, E., 1975. High-pressure decompositions in cobalt and nickel silicates. Phys. Earth Planet. Inter., 10, 88-93.

Ito, E. and Matsui, Y., 1977. Silicate ilmenite and the post-spinel transformations. In: Manghnani M.H. and Akimoto, S. (Eds.), High-Pressure Research: Applications in Geophysics. Academic Press, New York, pp. 193-208.

Kato, T. and Kumazawa, M., 1985. Garnet phase of $MgSiO_3$ filling the pyroxene-ilmenite gap at

very high temperature. Nature, 316, 803-805.

Kondo, T., Yagi, T., Syono, Y., Noguchi, Y., Atou, T., Kikegawa, T., and Shimomura, O., 2000. Phase transitions of MnO to 137 GPa. Journal of Applied Physics, 87, 4153-4159.

Kondo, T., Ohtani, E., Hirao, N., Yagi, T., and Kikegawa, T., 2004. Phase transitions of (Mg,Fe)O at megabar pressures. Phys. Earth Planet. Inter., 143-144, 201-213.

Liu, L., 1976. High-pressure phases of Co_2GeO_4, Ni_2GeO_4, Mn_2GeO_4 and $MnGeO_3$: implications for the germanate-silicate modeling scheme and the Earth's mantle. Earth Planet. Sci. Lett., 31, 393-396.

Mao, H.K., Xu, J., and Bell, P.M., 1986. Calibration of the ruby pressure gauge to 800 kbar under quasihydrostatic conditions. J. Geophys. Res., 91, 4673-4676.

Ming, L.C. and Bassett, W.A., 1975. Decomposition of $FeSiO_3$ into FeO + SiO_2 under very high pressure and high temperature. Earth Planet. Sci. Lett., 25, 68-70.

Murakami, M., Hirose, K., Ono, S., and Ohishi, Y., 2003. Stability of $CaCl_2$-type and α-PbO_2-type SiO_2 at high pressure and temperature determined by in-situ X-ray measurements. Geophys. Res. Lett., 30, 1207, doi:10.1029/2002GL016722.

Murakami, M., Hirose, K., Kawamura, K., Sata, N., and Ohishi, Y., 2004. Post-perovskite phase transition in $MgSiO_3$. Science, 304, 855-858.

Oganov, A.R. and Ono, S., 2004. Theoretical and experimental evidence for a post-perovskite phase of $MgSiO_3$ in Earth's D" layer. Nature, 430, 445-448.

Ono, S., Oishi, Y., and Mibe, K., 2004. Phase transition of Ca-perovskite and stability of Al-bearing Mg-perovskite in the lower mantle. Am. Mineral., 89, 1480-1485.

Ringwood, A.E., 1970. Phase transformations and the constitution of the mantle. Phys. Earth Planet. Inter., 3, 109-166.

Sata, N., Shen, G., Rivers, M.L., and Sutton, S.R., 2002. Pressure-volume equation of state of the high-pressure B2 phase of NaCl. Physical Review B, 65 (10), Art. No. 104114.

Shannon, R.D., 1976. Revised effective ionic radii and systematic studies of interatomic distances

in halides and chalcogenides. Acta Cryst., A32, 751-767.

Tateno, S., Hirose, K., Sata, N., and Ohishi, Y., 2006. High-pressure behavior of $MnGeO_3$ and $CdGeO_3$ perovsiktes and the post-perovskite phase transition. Phys. Chem. Miner., 32, 721-725.

Watanuki, T., Shimomura, O., Yagi, T., Kondo, T., and Issiki, M., 2001. Construction of laser-heated diamond anvil cell system for in situ X-ray diffraction study at SPring-8. Review of Scientific Instruments, 72, 1289-1292.

Table captions

Table 1. Transformation pressures of various silicate compounds to the perovskite phase at 1200 K.

Figure Captions

Fig. 1. X-ray diffraction patterns of the samples.

(a) $FeSiO_3$ at 117 GPa, 2100 K (λ = 0.4170 Å). Pressure was derived from the equation of state of Pt (Holmes et al., 1989). The phase assemblage of the sample is FeO (B1) + SiO_2 ($CaCl_2$-type). Lattice parameters determined from a few peaks are a = 3.846 Å for FeO (B1), and a = 3.960, b = 3.811, c = 2.489 Å for SiO_2 ($CaCl_2$-type). (b) $CaFeSi_2O_6$ at 149 GPa, 1800 K (λ = 0.4170Å). Pressure was derived from the equation of state of Pt (Holmes et al., 1989). The phase assemblage of the sample is $CaSiO_3$ perovskite + FeO (B1) + SiO_2 ($CaCl_2$-type). Lattice parameters determined from a very few peaks are a = 3.248 Å for $CaSiO_3$ perovskite, a = 3.782 Å for FeO (B1), and a = 3.889, b = 3.745, c = 2.463 Å for SiO_2 ($CaCl_2$-type). Coexistence of $CaCl_2$-type SiO_2 and α-PbO_2-type SiO_2 around this pressure is often reported (Murakami et al., 2003). (c) $MnSiO_3$ at 40 GPa, 1700 K (λ = 0.4177 Å). Pressure was derived from the equation of state of Au (Anderson et al., 1989). The existing phase of the sample is $MnSiO_3$ perovskite. The refined lattice parameters of $MnSiO_3$ perovskite are a = 4.7559(4), b = 4.8073(4), c = 6.7723(6) Å. (d) Co_2SiO_4 at 50 GPa, 300 K quenched from 2000 K (λ = 0.4151 Å). Pressure was derived from the equation of state of NaCl (B2) (Sata et al., 2002). The quenched phase assemblage of the sample is CoO (B1) + SiO_2 (stishovite). The refined lattice parameters are a = 4.002(1) Å for CoO (B1) and a = 3.983(1), c = 2.584(1) Å for stishovite. SC = SiO_2 ($CaCl_2$-type), SP = SiO_2 (α-PbO_2-type), FeO = FeO with a B1 structure, Ca-Pv = Ca-perovskite, MnPv = $MnSiO_3$ perovskite, CoO = CoO with a B1 structure, St = stishovite, B2 = NaCl with a B2 structure, Pt = platinum, Au = gold , Re = rhenium, Cor = corundum, ? = unknown or uncertain peak.

Fig. 2. Phase diagram of $MnSiO_3$ estimated from the product phases at high pressure and high

temperature.

Fig. 3. Schematic energy levels of 3d electrons for Fe^{2+} and Co^{2+} at the octahedral site of mono-oxides and at the distorted dodecahedral site of assumed perovskites. Note that the crystal field splitting at the octahedral site is larger than that at the distorted dodecahedral site (Burns, 1993). Also, the energy levels of the 3d electrons of Fe^{2+} and Co^{2+} at the distorted dodecahedral site of perovskites are further separated.

Fig. 4. Goldschmidt diagram of $A^{2+}B^{4+}O_3$ compounds which have a perovskite structure. This diagram was modified from Fig. 5 in Tateno et al. (2006) and the present results were added to the diagram. The horizontal axis is the ionic radius of the 6-coordinated B cation and the vertical axis is the ionic radius of the 8-coordinated A cation. The ionic radii are from Shannon (1976). The oblique lines indicate the tolerance factors (Goldschmidt, 1926). Solid circles: compounds which transform from orthorhombic perovskite to $CaIrO_3$-type post-perovskite with increasing pressure. Solid triangles: compounds which transform from perovskite to the other structure than $CaIrO_3$-type post-perovskite (Tateno et al., 2006). Compounds marked by solid symbols mean that their distortions increase with pressure, while compounds marked by open symbols mean that their distortions decrease with pressure. * (annotation: this should be replaced by the same symbol as that in the figure) = composition that does not procure perovskite in the ranges of pressure and temperature investigated.

Table 1

Transformation pressures of various silicate compounds to the perovskite phase at 1200 K

	Type of transformation	Transformation pressure (GPa)
$MgSiO_3$	ilmenite to perovskite	25[a]
$MnSiO_3$	garnet to perovskite	20
$CaSiO_3$	Ca_2SiO_4(larnite) + $CaSi_2O_5$ (titanite) to perovskite	13.5[b]
$FeSiO_3$	?	> 149?
$CoSiO_3$	?	> 79?

[a]Kato and Kumazawa, 1985

[b]Akaogi et al., 2004

(a)

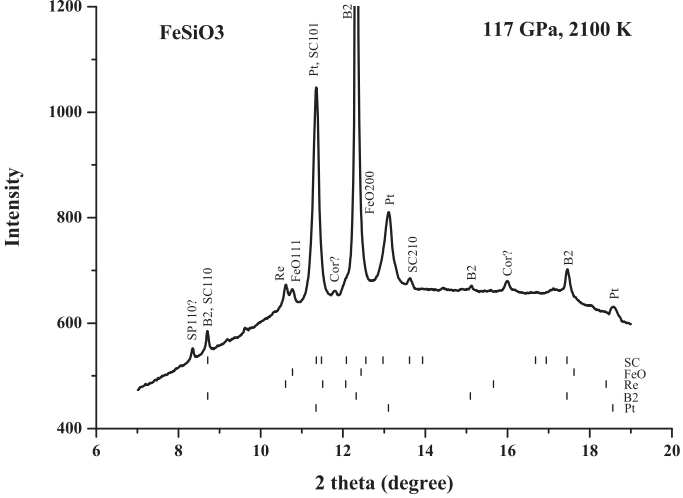
FeSiO3
117 GPa, 2100 K
Intensity
2 theta (degree)
SP110?
B2, SC110
Re
FeO111
Pt, SC101
Cor?
B2
FeO200
Pt
SC210
B2
Cor?
B2
Pt
SC
FeO
Re
B2
Pt

(b)

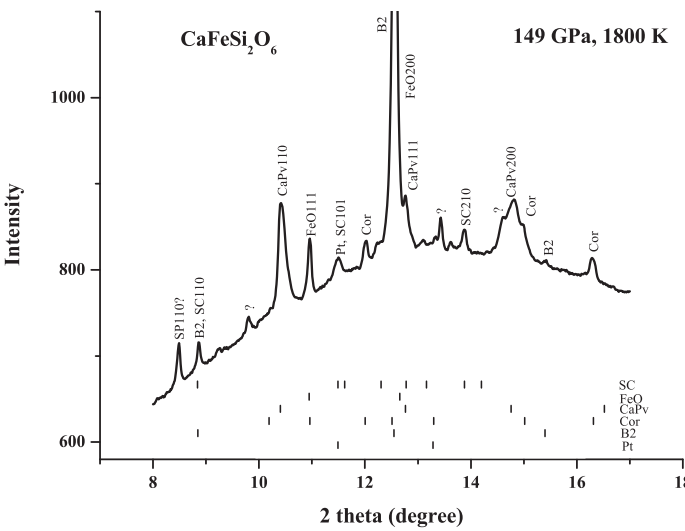
CaFeSi2O6
149 GPa, 1800 K
Intensity
2 theta (degree)
SP110?
B2, SC110
?
CaPv110
FeO111
Pt, SC101
Cor
B2
FeO200
CaPv111
?
SC210
?
CaPv200
Cor
B2
Cor
SC
FeO
CaPv
Cor
B2
Pt

(c)

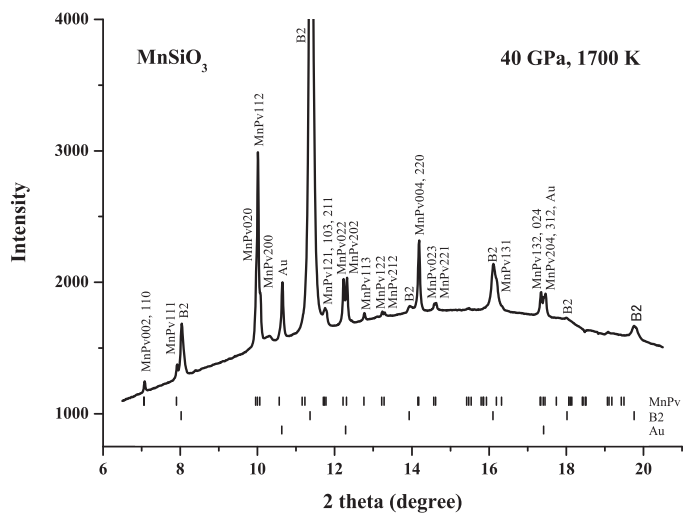
MnSiO3
40 GPa, 1700 K
Intensity
2 theta (degree)
MnPv002, 110
MnPv111
B2
MnPv020
MnPv112
MnPv200
Au
B2
MnPv121, 103, 211
MnPv022
MnPv202
MnPv113
MnPv122
MnPv212
B2
MnPv004, 220
MnPv023
MnPv221
B2
MnPv131
MnPv132, 024
MnPv204, 312, Au
B2
B2
MnPv
B2
Au

(d)

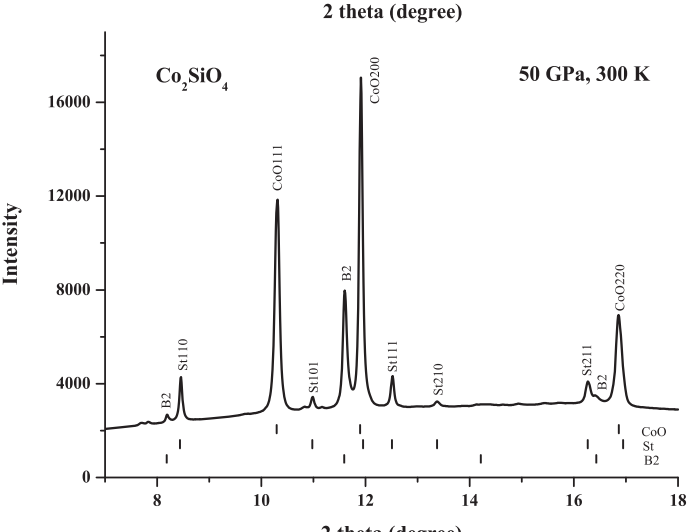
Co2SiO4
50 GPa, 300 K
Intensity
2 theta (degree)
B2
St110
CoO111
St101
B2
CoO200
St111
St210
St211
B2
CoO220
CoO
St
B2

Fig. 1

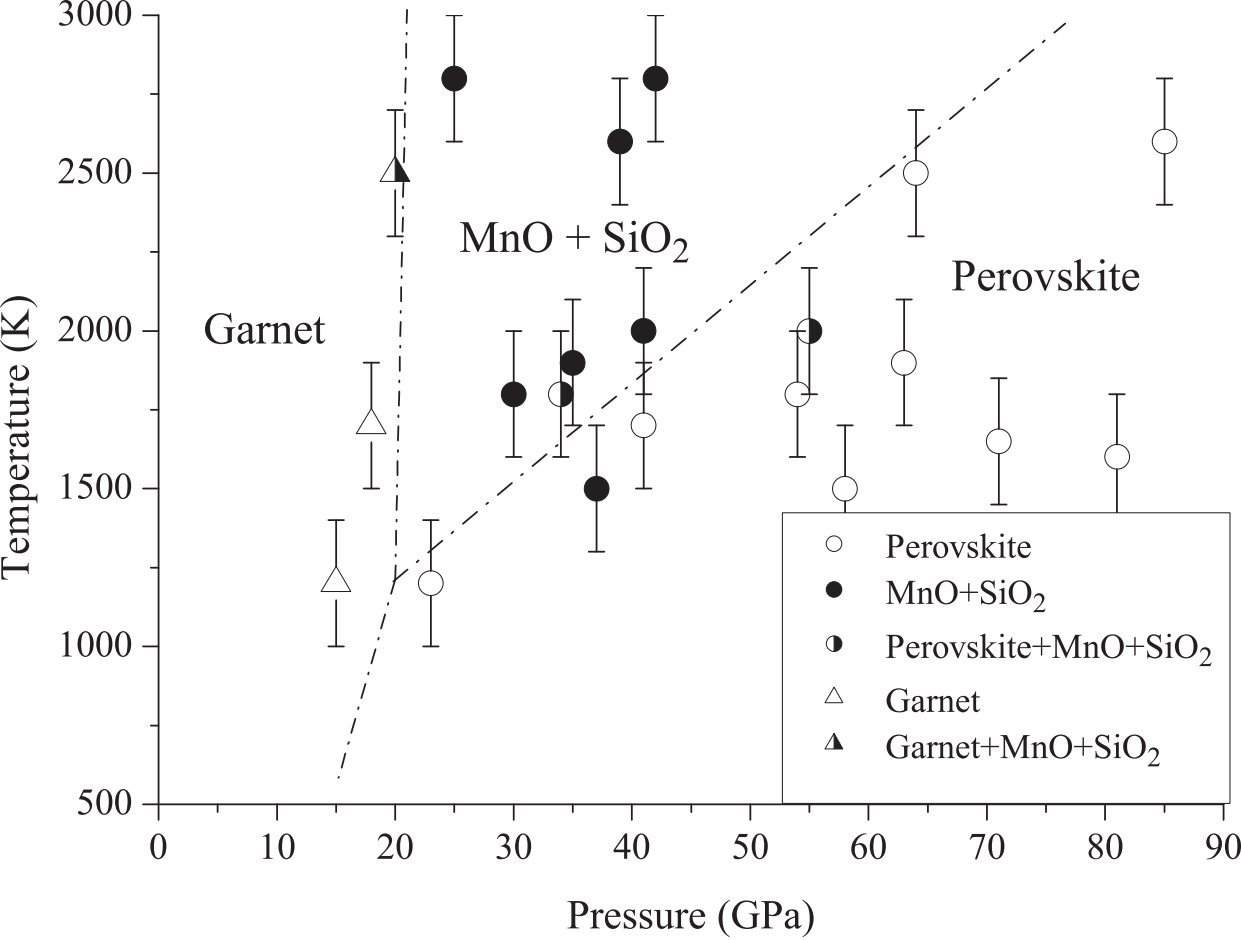
Garnet
MnO + SiO2
Perovskite
Temperature (K)
Pressure (GPa)
Perovskite
MnO+SiO2
Perovskite+MnO+SiO2
Garnet
Garnet+MnO+SiO2

Fig. 2

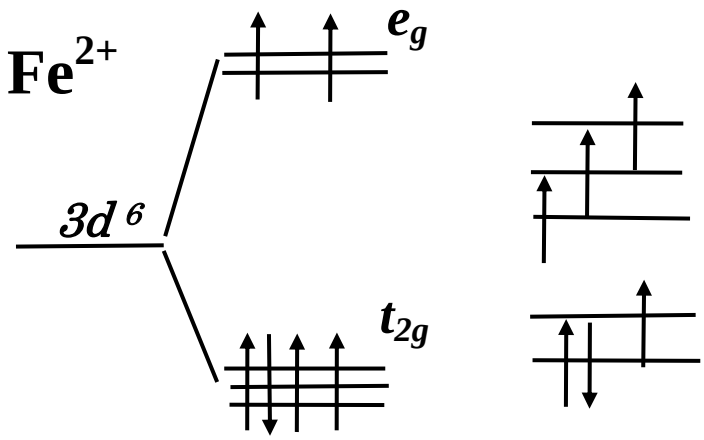

Octahedral Site of FeO **Dodecahedral site of perovskite**

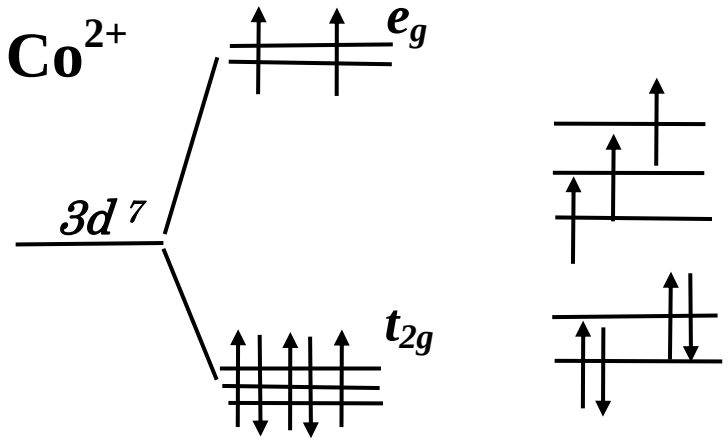

Octahedral Site of CoO **Dodecahedral site**

Fig. 3

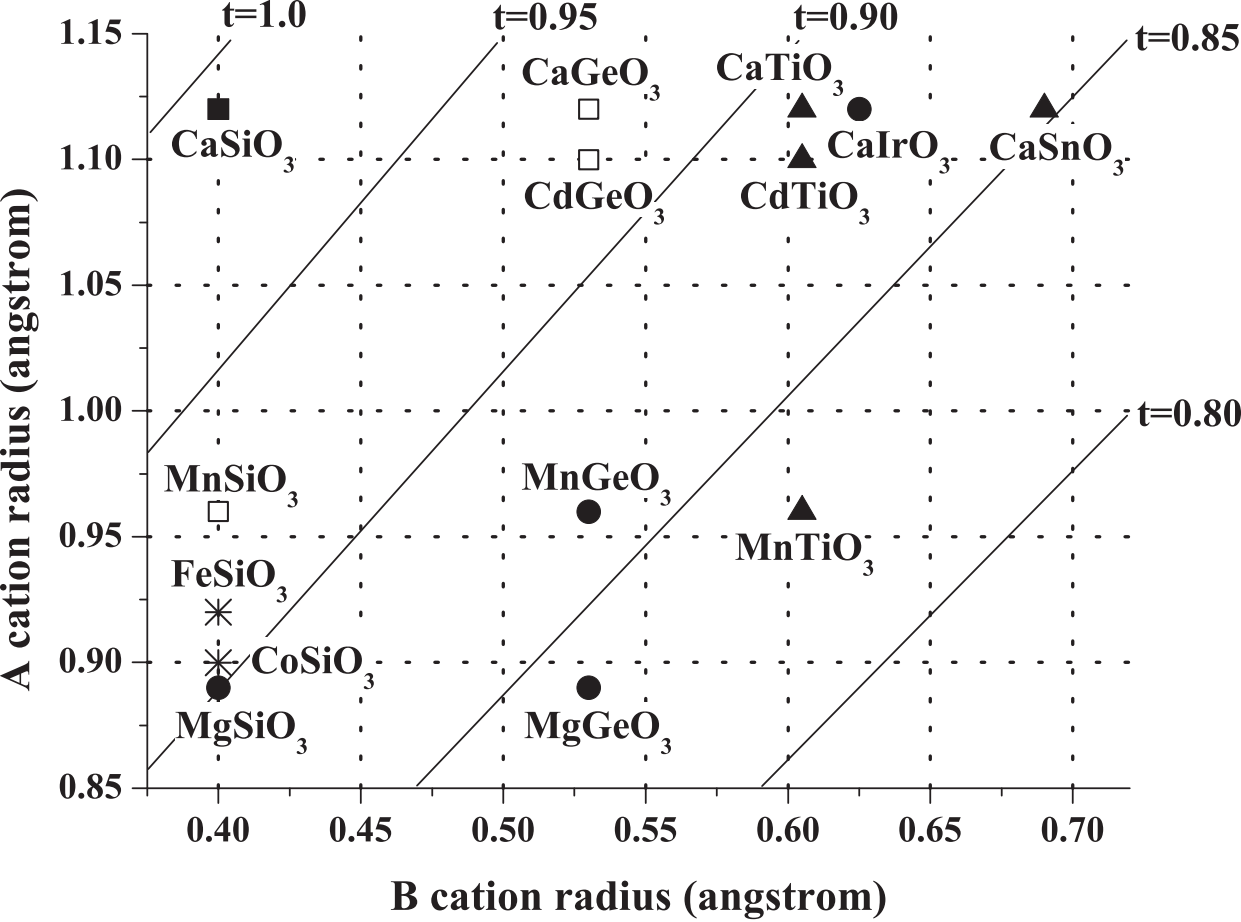
t=1.0
t=0.95
t=0.90
t=0.85
t=0.80
CaSiO3
CaGeO3
CaTiO3
CaIrO3
CaSnO3
CdGeO3
CdTiO3
MnSiO3
MnGeO3
MnTiO3
FeSiO3
CoSiO3
MgSiO3
MgGeO3
1.15
1.10
1.05
1.00
0.95
0.90
0.85
0.40
0.45
0.50
0.55
0.60
0.65
0.70
A cation radius (angstrom)
B cation radius (angstrom)

Fig. 4